Application of In-situ Attenuated Total Reflection-Fourier Transform Infrared Spectroscopy for the Understanding of Complex Reaction Mechanism and Kinetics: Formic Acid Oxidation on a Pt Film Electrode at Elevated Temperatures

Yan Xia Chen,*,† Shen Ye,‡ Martin Heinen,† Zenonas Jusys,† Masatoshi Osawa,‡ and R. Jürgen Behm*,†

Department Surface Chemistry and Catalysis, University of Ulm, D-89069 Ulm, Germany, and Catalysis Research Center, Hokkaido University, Sapporo 001-0021, Japan

Received: December 22, 2005; In Final Form: March 25, 2006

The potential of in-situ Fourier transform infrared (FTIR) spectroscopy measurements in an attenuated total reflection configuration (ATR-FTIRS) for the evaluation of reaction pathways, elementary reaction steps, and their kinetics is demonstrated for formic acid electrooxidation on a Pt film electrode. Quantitative kinetic information on two elementary steps, formic acid dehydration and CO_{ad} oxidation, and on the contributions of the related pathways in the dual path reaction mechanism are derived from IR spectroscopic signals in simultaneous electrochemical and ATR-FTIRS measurements over a wide temperature range (25−80 °C). Linearly and multiply bonded CO_{ad} and bridge-bonded formate are the only formic acid related stable reaction intermediates detected. With increasing temperature, the steady-state IR signal of CO_{ad} increases, while that of formate decreases. Reaction rates for CO_{ad} formation via formic acid dehydration and for CO_{ad} oxidation as well as the activation energies of these processes were determined at different temperatures, potentials, and surface conditions (with and without preadsorbed CO from formic acid dehydration) from the temporal evolution of the IR intensities of CO_{ad} during adsorption/reaction transients, using an IR intensity−CO_{ad} coverage calibration. At potentials up to 0.75 V and temperatures from 25 to 80 °C, the "indirect" CO pathway contributes less than 5% (at potentials ≤0.6 V significantly below 1%) to the total Faradaic reaction current, making the "direct" pathway by far the dominant one under the present reaction conditions. Much higher activation energies for CO_{ad} formation and CO_{ad} oxidation compared with the effective activation energy of the total reaction, derived from the Faradaic currents, support this conclusion.

1. Introduction

The thermal activation of chemical reactions is one of the most general, fundamental issues in chemistry, controlling the reaction rate as well as, in more complex reaction processes, the amount and distribution of different reaction products or byproducts. In the current contribution, we report results of a combined electrochemical and in-situ infrared spectroscopy study, in an attenuated total reflection (ATR) geometry,[1,2] on the electrooxidation of formic acid on a Pt film electrode, where we are particularly interested in temperature-dependent variations in the nature and coverage of adsorbed reaction intermediates and in the contributions of different reaction pathways to the total reaction kinetics, over a temperature range of 25−80 °C. In these measurements, we make use of the high surface sensitivity of ATR-FTIRS and in particular of its ability to work also in bulk electrolyte, which largely reduces artifacts resulting from mass transport limitations and reactant depletion as encountered in the commonly used external reflection thin-layer configuration.[3]

Formic acid oxidation has attracted considerable interest in the past 40 years, both as a model system for understanding the mechanism of the electrooxidation of small organic molecules and because of its technical relevance for fuel cell applications (see, e.g., refs 4−12), where formic acid is one of the intermediate products in direct methanol fuel cells (DMFCs)[13−17] and was proposed also as a fuel for a direct formic acid fuel cell for portable applications.[18,19] To reduce the kinetic limitations, these fuel cells are mostly operated at elevated temperatures, around or above 80 °C. Therefore, a detailed understanding of temperature effects on the mechanism and kinetics of formic acid oxidation is highly important. So far, most of the investigations on formic acid oxidation reported have been carried out at room temperature, and information on the reaction behavior at elevated temperatures is sparse (see below).[20−26] The present mechanistic understanding of formic acid oxidation on Pt as derived from these studies can be summarized as follows: It is generally accepted that this reaction proceeds via the so-called "dual path" mechanism.[4−6,27,28] In the indirect pathway, formic acid, most likely an adsorbed, molecular $HCOOH_{ad}$ species, is first dehydrated to form adsorbed CO_{ad}, which is then oxidized to CO_2, while in the direct pathway, formic acid oxidation proceeds "directly" via one or several reactive intermediates to CO_2, without the formation of CO_{ad}.[5−11,27] This mechanistic assignment was initially based on the observation that formic acid oxidation was possible at potentials significantly cathodic of the onset potential for CO_{ad} oxidation.[4−6] It is important to note that the direct reaction pathway, via a reactive intermediate, does not require an external oxygen source such as adsorbed OH, in contrast to

* To whom correspondence should be addressed. E-mail: yan-xia.chen@uni-ulm.de; juergen.behm@uni-ulm.de. Fax: xx49-731-50-25452.

† University of Ulm.

‡ Hokkaido University.

10.1021/jp057463h CCC: $33.50
Published on Web 04/26/2006

the indirect pathway, which explains the observation that formic acid oxidation could occur at more negative potentials than required for H_2O dissociation on Pt (>0.4 V).[5,29−31] The first definitive evidence for the non-CO_{ad} pathway came from a differential electrochemical mass spectroscopic study (DEMS) involving isotope-labeled reactants,[29] which showed $^{12}CO_2$ formation before any $^{13}CO_2$ formation, when a surface covered by a "saturated" ^{13}CO adlayer was exposed to unlabeled HCOOH.[32] Finally, Weaver and co-workers concluded from the slow CO_{ad} formation rate on Pt (by HCOOH dehydration) at 0.35 V and from the absence of $^{13}CO/^{12}CO$ isotope exchange (in $H^{12}COOH$, after presaturation with $^{13}CO_{ad}$ from $H^{13}COOH$) that the formation and oxidation of CO_{ad} cannot be the dominant reaction pathway for formic acid oxidation on Pt under these conditions but could not rule out a more significant contribution at higher potentials.[33] The chemical nature of the reactive intermediates and details on the elementary reaction steps, however, remained controversial.

Information on the nature of possible reaction intermediates was obtained from in-situ IR studies. Obvious alternative chemisorbed intermediates besides CO_{ad} are formate $HCOO_{ad}$, COH_{ad}, CHO_{ad}, or $COOH_{ad}$. A weak band at 1262 cm^{-1} assigned to C−OH was reported by Xia et al.,[34] and Sun et al. reported a very weak IR band at ca. 1735 cm^{-1}, which they tentatively attributed to a $COOH_{ad}$ species.[35] These signals, however, were not observed in other studies.[36−38] Very recently, two in-situ IR studies reported the observation of an adsorbed formate species with a band at 1320 cm^{-1} (symmetric OCO stretch vibration) during electrochemical formic acid oxidation on Ir[39] and Pt,[40] which, based on the absence of the corresponding anti-symmetric stretch vibration, was suggested to be adsorbed in a bridge-bonded configuration, with two oxygen atoms bound to the Pt surface.[40,41] The above adsorbates have been proposed to act as reactive intermediates in the direct pathway of formic acid oxidation by those authors. Since similar formate species were observed also during electrooxidation of methanol and formaldehyde on a Pt electrode,[42,43] it was suggested that formate operates as the reactive intermediate also during methanol and formaldehyde oxidation. The role of the adsorbed formate was further investigated in two recent studies of our groups.[44,45]

Most of these studies have been performed at room temperature. The few previous studies carried out at elevated temperatures showed an increase in the formic acid oxidation rate with increasing temperature,[22,24,46−50] a cathodic shift in the onset potential for formic acid oxidation on Pt, down to 0.2 V_{RHE} at 150 °C,[25] and the formation of CO_2 as the only reaction product also at elevated temperatures in a formic acid operated polymer electrolyte fuel cell at 170 °C.[21] In-situ IR measurements performed in a thin-layer geometry resolved linearly bonded CO_{ad} as a stable, adsorbed reaction intermediate on a Ru(0001) electrode in the temperature range of 10 to 50 °C.[26] Finally, very little is known on the relative contributions of the different reaction pathways to the formic acid oxidation reaction at elevated temperatures.

In the following, we will, after a brief description of the experimental setup and procedures, first present and discuss the results of potentiodynamic experiments, including simultaneous electrochemical and in-situ IR measurements in the temperature range between 25 and 80 °C. More direct kinetic information is obtained from potentiostatic potential-step experiments in the same temperature range, which are described in the following section. Finally, we derive reaction rates, turnover frequencies (TOFs), and activation energies of two different elementary reactions involved in formic acid oxidation, CO_{ad} formation via HCOOH dehydration and CO_{ad} oxidation, from these transient electrochemical and IR measurements under different reaction conditions and discuss the contribution of the indirect and direct pathways to the total reaction process under the present reaction conditions.

2. Experimental Section

The spectroelectrochemical cell used in these measurements was similar to that used in previous studies in the Osawa group,[51] except for an additional glass jacket that allowed water to circulate around the cell to control the cell temperature. A thin Pt film (thickness 50 nm), which was prepared by electroless Pt deposition on the reflecting flat surface of a hemicylindrical Si prism following procedures described elsewhere,[40,43] was used as the working electrode. The roughness factor of these film electrodes was around 10, as determined from the hydrogen adsorption and desorption charge and from the CO_{ad} stripping charge. Current densities were normalized to the active surface area determined this way. A Pt gauge and a reversible hydrogen electrode (RHE) served as the counter and reference electrodes, respectively. The reference electrode was kept at room temperature during the elevated temperature measurements; all potentials in this study are quoted against RHE. The deviation introduced by keeping the reference electrode at room temperature is within a few millivolts and thus on the order of the experimental error.

All electrolyte solutions were prepared using Millipore water (18.2 MΩ) and 0.5 M H_2SO_4 as the supporting electrolyte. Formic acid (analytical grade, Merck) and H_2SO_4 (suprapure, Merck) were used without further purification. Before the measurements, the Pt thin-film electrode was cycled between 0.05 and 1.3 V in 0.5 M H_2SO_4 solution, until the characteristic features of hydrogen adsorption/desorption and oxide formation/reduction for polycrystalline Pt were reproduced. Then the solution in the IR spectroscopic cell was replaced by a freshly prepared 0.5 M H_2SO_4 + 0.1 M HCOOH solution and purged with Ar for ca. 60 min, before performing the spectroelectrochemical measurements. In the potential-step transient experiments, the electrode was first held for 10 min at 0.05 V or for 1 min at 1.2 V before stepping to the respective reaction potential, to ensure that the steady-state adlayer composition was reached (0.05 V) or that oxidizable species were completely removed (1.2 V).

The in-situ IR measurements were carried out in a BioRad FTIR-6000 spectrometer equipped with a MCT detector. All spectra were obtained at a resolution of 4 cm^{-1} (25 co-added scans per spectrum, 5 s per scan set) during potentiodynamic measurements and 5 scans per spectrum (1 s per spectrum) in potential-step transients. The IR intensities are plotted as absorbance, that is, $\log(R_0/R)$, where R_0 and R describe the reflectance at the reference potential and sample potential, respectively. This data processing results in spectra with peaks pointing up for increased absorption ($R < R_0$) and peaks pointing down for a decrease in absorption ($R > R_0$). The IR spectra were normalized to a spectrum recorded at 1.2 V in formic acid containing electrolyte, after holding the potential at 1.2 V for 1 min prior to the measurements. This procedure ensures the complete removal of formic acid related surface adsorbates from the surface.

3. Results

3.1. Cyclic Voltammetry and In-situ IR Measurements. A typical base voltammogram (CV) of the Pt thin-film electrode

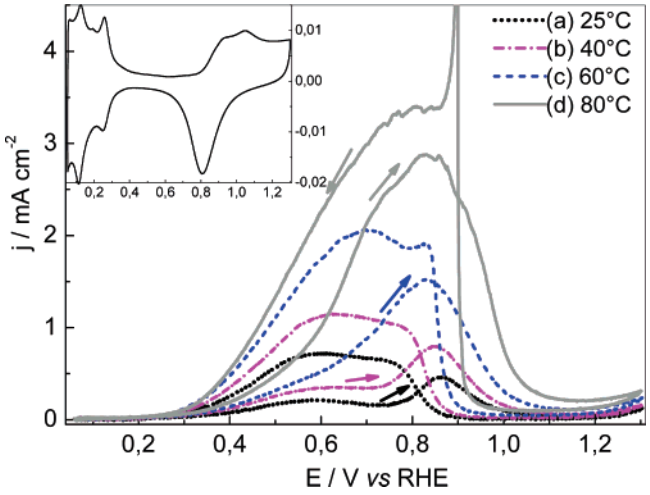

Figure 1. Cyclic voltammograms of the Pt thin-film electrode in 0.1 M HCOOH + 0.5 M H_2SO_4 at different temperatures (a) 25 °C, (b) 40 °C, (c) 60 °C, and (d) 80 °C. Inset: cyclic voltammogram of the Pt thin film in supporting electrolyte, scan rate, 10 mV s^{-1}.

in 0.5 M H_2SO_4 in the potential range from 0.05 to 1.3 V (scan rate 10 mV·s^{-1}) is shown in the inset of Figure 1. It resembles that obtained on polycrystalline Pt electrodes,[52] confirming that the thin-film Pt electrode has essentially the same electrochemical properties as a polycrystalline Pt electrode. Representative CVs of the Pt film in contact with 0.1 M HCOOH + 0.5 M H_2SO_4 solution at 25, 40, 60, and 80 °C (scan rate 10 mV·s^{-1}) are shown in the main body of Figure 1. While the general shape of the CVs is quite similar for the different temperatures, the anodic current and the potential window for bulk oxidation increase significantly with temperature, together with a decrease of the ignition potential for formic acid bulk oxidation. The cathodic shift of the ignition potential indicates that the reactivity of the Pt electrode toward formic acid oxidation is significantly enhanced by thermal activation. At 25 °C, we find an appreciable anodic current flow at potentials higher than 0.30 V in the positive-going scan, with a low-current pre-peak in the potential region from 0.30 to 0.75 V ("peak I") peak center at ca. 0.55 V, which is followed by a symmetric current peak ("peak II") centered at ca. 0.88 V. The current increase from 0.30 to 0.55 V is attributed to an electrochemical activation of the HCOOH oxidation; sulfate or water adsorption have been made responsible for the current decay from 0.55 to 0.75 V, for example, by Markovic et al. and Iwasita et al.,[53,54] but other processes such as OH or formate adsorption cannot be ruled out either.[45,55] Peak II in the CV is attributed to both CO_{ad} and bulk formic acid oxidation,[56] where the former is evidenced also by the decrease in the CO_{ad} related IR intensities in this potential range. At even more anodic potentials, the current remains at very low values due to Pt-oxide formation until close to the most anodic potential, at >1.2 V, where it starts to increase again. In the negative-going scan, the anodic current decays rapidly and then remains at very low values down to around 0.85 V, reflecting the low activity of oxidized Pt for formic acid oxidation. Starting from 0.85 V, the current increases rapidly due to PtO_x reduction, followed by a current plateau from 0.75 to 0.5 V ("peak III").[50] Note that the current in this potential range is more than four times higher than that at the same potential in the positive-going scan. Below 0.5 V, the current decreases and drops to nearly zero at potentials below 0.2 V, which was associated with surface poisoning due to CO_{ad} accumulation[36,57] (see also the IR results presented below). The considerable hysteresis and the significant difference in the shape of the $I-U$ curves between the positive-going and negative-going scans are generally attributed to the hysteresis in the formation and reduction of the surface oxide in the high potential range and to the time required for the oxidation or build-up of the poisoning CO adlayer in the low potential range.[50,52,54,58]

For higher temperatures, the main current peak in the positive-going scans (peak II) maintains a bell-shape with the peak potential slightly decreasing from 0.88 V (25 °C) to 0.82 V (80 °C). The peak current increases by a factor of 2 (40 °C), 4 (60 °C), or 6 (80 °C) compared with the maximum current at 25 °C. At the higher temperatures, 60 and 80 °C, the pre-peak (peak I) is not resolved as a separate feature anymore, but incorporated into the main peak, leaving the onset for reaction at about 0.3 V. Also, in the negative-going scan, the current largely follows the shape of the CV recorded at 25 °C, but the ignition potential for formic acid bulk oxidation, which is coupled to the reduction of the surface oxide produced in the previous positive-going scan, shifts to more positive values with higher temperature, from ca. 0.85 V at 25 °C to about 0.95 V at 80 °C. Furthermore, the initial current develops into a sharp peak, which is likely to result from Ohmic drop effects,[50] and the current plateau ("peak III") becomes narrower at higher temperatures.

Simultaneously with measuring the CVs in-situ IR spectra were recorded in increments of 50 mV (Figure 2). Except for small differences in the band frequency and intensity as well as in the potential region for the appearance/disappearance of those bands, the sets of spectra recorded at higher temperatures are qualitatively very similar to the spectra taken at 25 °C (Figure 2a). No new bands were observed at the higher temperatures. Therefore, only two representative sets taken at 25 and 80 °C are shown here (parts a and b of Figure 2). For better identification of small changes in the peak shapes and frequencies, selected spectra recorded at 0.3, 0.6, and 0.8 V in the positive-going and at 0.3 and 0.6 V in the negative-going scans are displayed in parts c and d of Figure 2.

The two positive bands with peaks at ca. 2080 and 1850 cm^{-1} are attributed to linearly bonded CO_{ad} (CO_L) and multifold-bonded CO_{ad} (CO_M), respectively. A rather narrow, weak signal centered at ca. 1322 cm^{-1} is assigned to formate ($HCOO_{ad}$) in a bridge-bonded configuration bound via two oxygen atoms to the Pt surface.[40−42,59,60] Additional weak bipolar bands around 1620 cm^{-1} and above 3000 cm^{-1} arise from potential-induced changes in the water adlayer together with the displacement of water due to CO and formate adsorption, while those below 1300 cm^{-1} are assigned to sulfate/bisulfate displacement (see Figure 2), both, of adsorbed species and anions in solution close to the electrode surface.[3,61] No other bands besides those mentioned above have been observed in the present study.

The corresponding potential-dependent band changes in the intensities of adsorbed CO_{ad} and formate at different temperatures are evaluated and plotted in Figure 3. We will start the discussion of the potential dependence using the curves at 25 °C. In the potential region from 0.05 to 0.4 V, the intensity of the CO_L species increases slightly, while that of the CO_M species decreases. At more anodic potentials, both bands show a slight decrease with potential. The small intensity increase in the CO_L signal from 0.05 to 0.40 V is partly explained by a potential-induced redistribution of some of the CO_{ad} species (CO_M to CO_L),[38] plus additional CO_{ad} due to increasing exposure. (Waiting times of almost 10 min were found to be necessary, e.g., to ensure full saturation of the electrode at 0.05 V and 25 °C.) The decrease of the CO_{ad} intensity from 0.40 to 0.7 V is attributed to the onset of CO_{ad} oxidation (indirect HCOOH

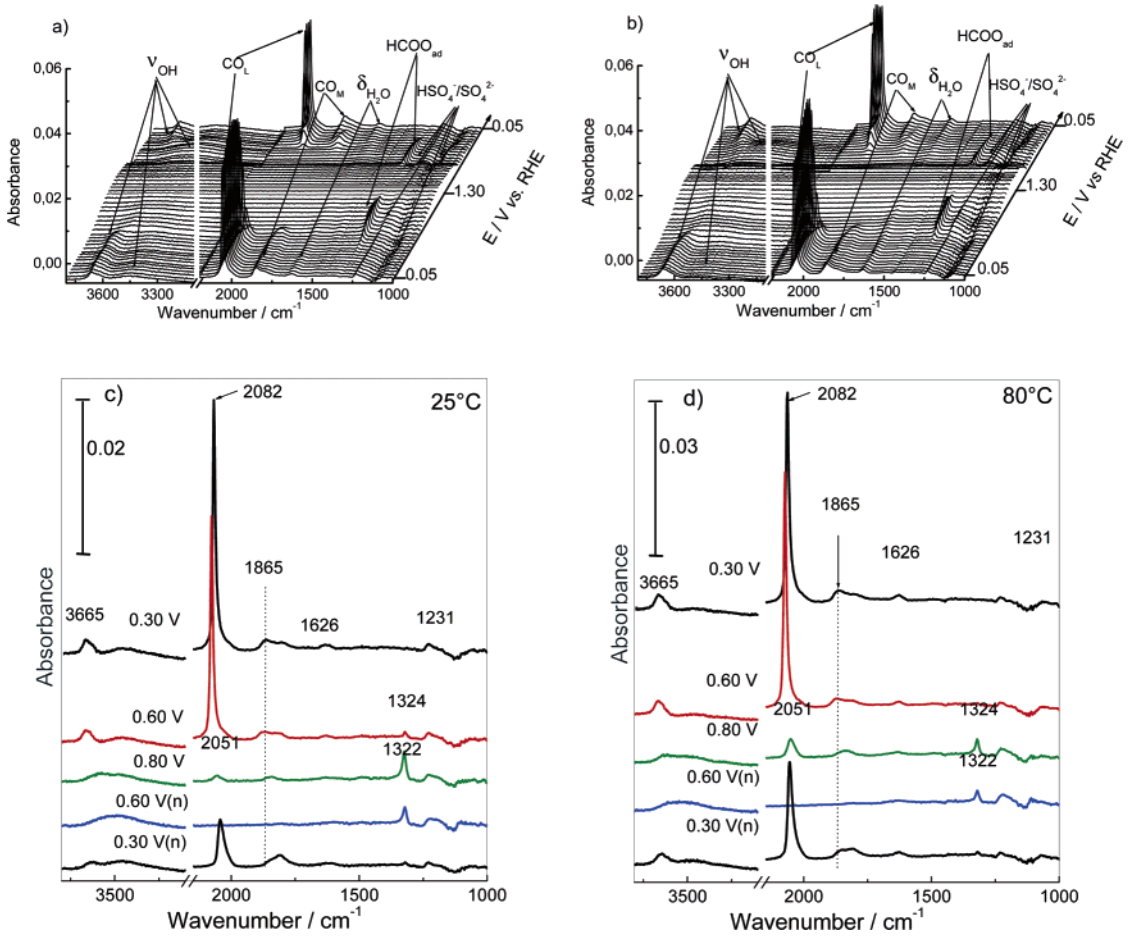

Figure 2. IR spectra of the interface during HCOOH oxidation on a Pt thin-film electrode in 0.5 M H_2SO_4 and 0.1 M HCOOH solution at (a) 25 °C and (b) 80 °C. Selected spectra recorded at 0.3, 0.6, and 0.8 V in the positive-going and 0.6 and 0.3 V in the negative-going scans (denoted as (n) in the figure) at (c) 25 °C and (d) 80 °C. The potential was scanned from 0.05 to 1.3 V and then back to 0.05 V; the corresponding CV is shown in Figure 1. Twenty-five interferograms were co-added to each spectrum; the background spectrum was recorded at 1.2 V.

oxidation),[56] although the pre-peak observed in the CV ("peak I") is primarily attributed to a process other than CO_{ad} oxidation. This will be discussed in more detail in section 4. At potentials higher than 0.7 V, the CO_{ad} intensity decreases sharply, together with the increase of the anodic current (Figure 1a). The CO_{ad} bands disappear completely at potentials higher than 0.85 V, where the surface oxide starts to form. Peak II in the CV can be assigned to the oxidation of both CO_{ad} and formic acid from the bulk.[56] The relative contributions of these two reactions will be discussed in section 4.

In the negative-going potential scan, both CO_{ad} bands, CO_L and CO_M, reappear only at potentials below 0.55 V (Figures 2 and 3), while the onset of the Faradaic current occurs at about 0.85 V (Figure 1). Hence, in the potential range between 0.85 and 0.55 V, the dehydration of formic acid to CO_{ad} seems to be significantly slower than the CO_{ad} oxidation rate in this potential range. Only at more cathodic potentials, below 0.55 V, does the CO_{ad} oxidation rate become sufficiently slow enough that the build-up of a CO adlayer becomes feasible. (It should be noted that because of the convolution of time and potential effects in potentiodynamic experiments these potential values are only approximate. More precise values are obtained from the potentiostatic potential-step experiments described in the following section.) Interestingly, the absence of CO_{ad} on the surface at potentials between 0.85 and 0.55 V coincides with the broad current plateau (peak III). The constant and significant Faradaic current between 0.85 and 0.55 V in combination with the strong increase of the CO_{ad} oxidation rate from 0.55 to 0.85 V indicates already that the contribution from the indirect, CO_{ad} related pathway cannot be dominant.

The intensity of the CO_L band increases sharply upon further decreasing the potential from 0.45 to 0.2 V (Figures 2 and 3), followed by a slow decrease of the CO_L signal down to 0.05 V. Also, the CO_M intensity increases significantly at potentials from 0.55 to 0.35 V, followed by a slower increase in intensity at the more cathodic potentials discussed above. The opposing trends in CO_L and CO_M changes in the potential range between 0.35 and 0.05 V—decrease in CO_L intensity and increase in CO_M intensity—support our explanation of a redistribution of the CO_{ad} species in the low potential regime given above. The accumulation of CO_{ad} on the surface at $E < 0.45$ V increasingly blocks the surface and hence results in the steep decrease of the anodic current.

The formate band appears at ca. 0.4 V in the positive-going scan, increases slowly from 0.4 to 0.7 V, and then grows steeply from 0.7 V to the current peak at about 0.9 V (Figures 2 and 3c). It is important to note that the increase in formate coverage coincides with the decrease in CO_{ad} coverage. At potentials higher than 0.9 V, the intensity of the formate peak decreases and reaches zero at around 1.2 V, which we associate with surface oxide formation. In the backward potential scan, the formate band reappears at ca. 0.9 V and increases sharply in intensity, reaching its maximum at 0.7 to 0.65 V. The hysteresis between formate removal in the positive-going scan and formate formation in the negative-going scan is related to the hysteresis in formation and reduction of OH_{ad} and PtO_x species on the

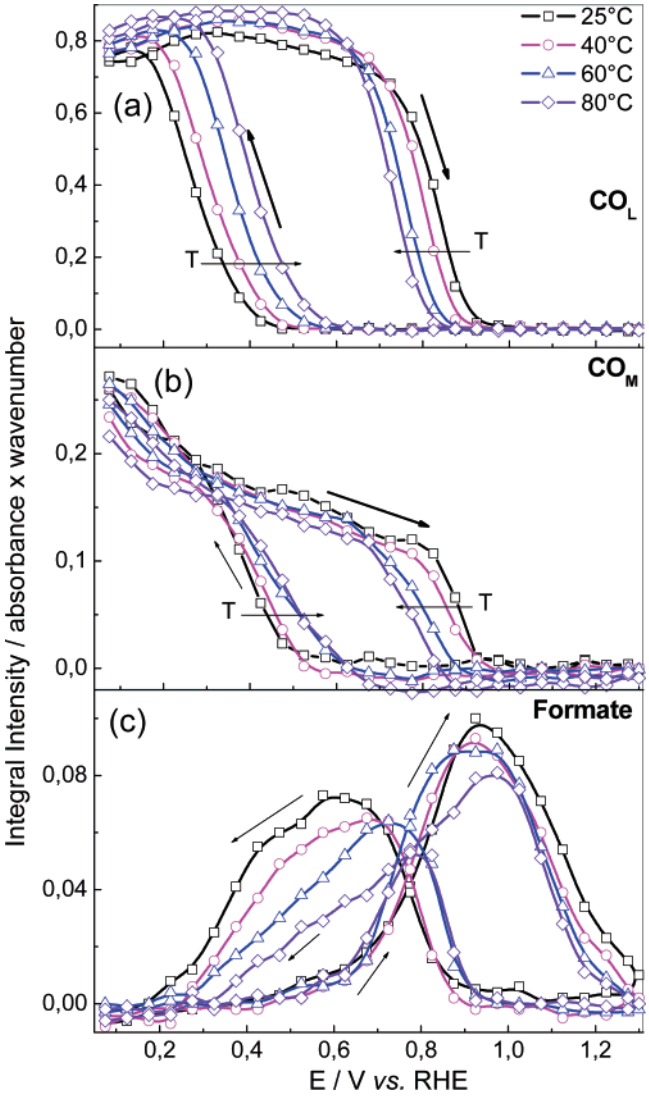

Figure 3. Dependence of the integral band intensity of (a) CO_L, (b) CO_M, and (c) formate on the electrode potential and temperature. Other conditions are the same as those in Figures 1 and 2.

surface.[52] Further lowering of the potential leads to an intensity decrease and finally disappearance of the signal at potentials at 0.2 V, which is related to both the decreasing adsorption energy and the growing CO_{ad} coverage.

Temperature effects on the IR band intensities are illustrated by the plots of the potential-dependent integral band intensities of the spectra taken at 25, 40, 60, and 80 °C in Figure 3. The general shapes of the potential-dependent band intensities for both adsorbed CO and formate do not change significantly with temperatures. The characteristic changes in adsorbate coverages described above, however, are shifted in potential (see arrows in Figure 3), resulting in the following trends:

(i) With higher temperature, the CO_L band intensities at the same potential increase slightly in the range between 0.05 and 0.7 V, while the CO_M intensity decreases. Furthermore, the potential for the abrupt decay of the CO_{ad} band intensity decreases with higher temperature. These shifts reflect a thermal activation of the formic acid dehydration and CO_{ad} oxidation reactions.

(ii) In the negative-going scan, the reappearance of CO_{ad} shifts anodically with temperature. It is known that the reduction of Pt oxide can take place both electrochemically and chemically, for example, by reaction with formic acid.[62−65] The temperature effect suggests that also these processes are thermally activated.

(iii) Though the potential-dependent formate band profiles are quite similar at all four temperatures and largely follow the shape of the CVs, their absolute intensities behave opposite to the Faradaic current signal, that is, they decrease with higher temperature, in particular in the negative-going potential scan. A similar decrease of the formate band intensity with temperature was observed also in a study on the electrooxidation of methanol and formaldehyde.[66] Possible correlations between the large increase in anodic current and the decrease of the formate band intensity with temperature will be given in section 4.

The electrochemical and in-situ IR spectra presented so far can be summarized as follows: (i) CO_{ad} and adsorbed formate are the only formic acid related adsorbates detected by ATR-FTIRS in the entire potential and temperature range investigated; (ii) the formate band intensity decreases with increasing temperature; (iii) the rates of formic acid dehydration (CO_{ad} formation) and formic acid oxidation increase with temperature.

3.2. Potentiostatic Electrochemical and In-situ IR Measurements. The convolution of potential and time effects in the potentiodynamic sweep experiments renders a quantitative determination of quantities such as the onset potential difficult. More direct kinetic information is obtained from potentiostatic measurements, following the change of adsorbate coverage with time and its correlation with the anodic current. We therefore performed combined chronoamperometric and time-dependent ATR-FTIRS measurements, following the temporal evolution of anodic current and adlayer composition/coverage at constant potentials of 0.5, 0.6, and 0.75 V at different temperatures (25, 40, 60, and 80 °C). These three potentials were selected to cover the main reaction regime with measurable CO_{ad} oxidation rates. The experiments were performed in two different ways, either by holding the potential at 1.2 V for 1 min and then stepping to the respective reaction potential or by stepping from 0.05 V, where the electrode was held for 10 min, to the reaction potential. In the former case, the surface is free of adsorbed CO and formate species; in the latter case, the electrode is precovered by 0.52 ML CO_{ad} due to dissociative adsorption (dehydration) of formic acid at the initial anodic potential of 0.05 V.[44] (Note that adsorption can take place not only while holding the potential at 0.05 V but also in the preceding negative-going scan.)

The $I-t$ curves resulting from these potential-step experiments at different temperatures and reaction potentials are displayed in Figure 4. Representative sets of time-dependent IR spectra in the region from 1000 to 2150 cm^{-1}, collected after stepping the potential from 0.05 to 0.6 V (parts a and c of Figure 5) and from 1.2 to 0.6 V (parts b and d of Figure 5) at 60 °C, respectively, are shown in Figure 5; plots of the integrated intensities of the CO_L, CO_M, and formate bands as a function of time at all four temperatures are presented in Figure 6. Similar to the potentiodynamic measurements, no formic acid related adsorbed intermediates other than CO_{ad} and bridge-adsorbed formate are observed. After stepping the potential from 0.05 to 0.5 V, at 25 and 40 °C the anodic current first jumps to a maximum and then decays slowly with time. In contrast, at 80 °C reaction temperature, and, less pronounced, also at 60 °C, the anodic current increases again slowly with time, after having passed through the initial maximum and the subsequent current decay (Figure 4). The IR spectra show that, at 0.5 V reaction potential and 25 and 40 °C, there is a slight increase of the CO_L band intensity accompanied by a decrease of the CO_M band

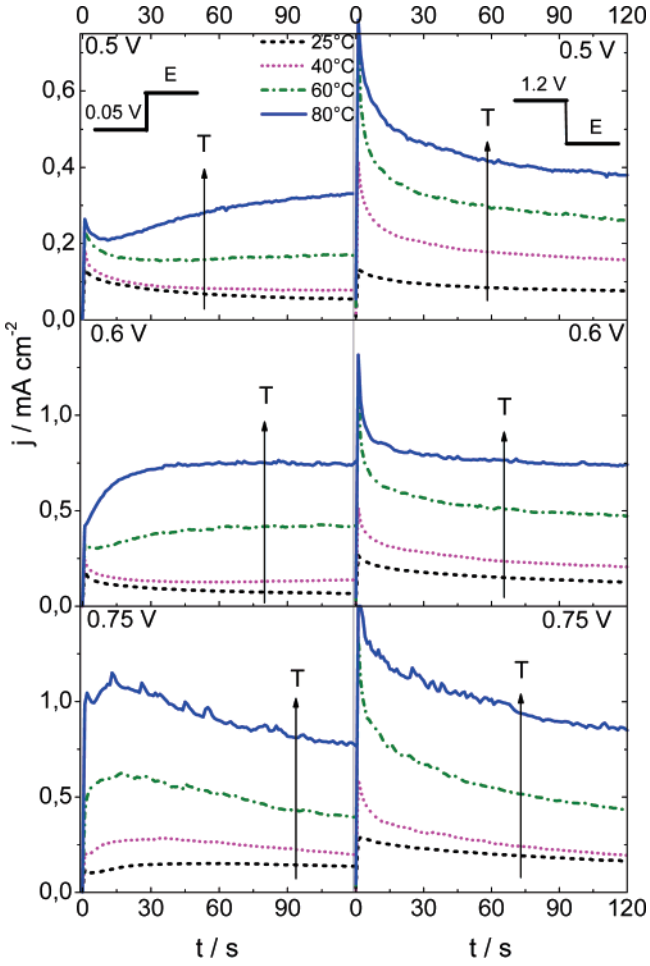

Figure 4. Chronoamperometric transients during potentiostatic oxidation of HCOOH on a Pt electrode at four different temperatures (25, 40, 60, and 80 °C) following a potential step from 0.05 V (left) and from 1.2 V to the respective reaction potential. Pretreatment as described in the text.

intensity within the first few seconds after the potential step, reflecting some conversion from CO_M to CO_L.[38] Subsequently, the intensities do not change with time (Figures 4 and parts a and b of Figure 6). At 40, 60, and 80 °C, the CO_L band intensities decrease with the current increase, with the decay at 80 °C being more pronounced than at 60 and 40 °C (Figures 4 and parts a and b of Figure 6), reflecting an increasing net rate for CO_{ad} removal with temperature. The intensity of the CO_M band is much weaker than the CO_L signal and also varies much less with temperature and time (Figure 6b), except for the initial abrupt decrease along with the potential step due to the potential-induced change in adsorption site, from CO_M to CO_L (see previous section). The formate band intensity is barely detectable at this potential for all four temperatures (Figure 6c).

By stepping the potential from 0.05 to 0.6 V, the current densities are slightly higher than those at 0.5 V (Figure 4). Correspondingly, the CO_L intensity decreases much faster than at 0.5 V and the CO_M signal also shows an appreciable intensity decrease with time. Hence, at 0.6 V, CO_{ad} oxidation is already significant compared with CO_{ad} formation, especially at higher temperatures. On the other hand, a weak formate band appears right after the potential step to 0.6 V (Figure 6c). Its intensity hardly changes with time and temperature. At 0.75 V reaction potential, the CO_{ad} band intensity decreases much faster than at 0.5 and 0.6 V. The CO_L signal disappears within 45 s after the potential step from 0.05 to 0.75 V at all four temperatures. The CO_M intensity decreases at a slower rate than that of CO_L, but 2 min after the potential step, the CO_M intensity is also much weaker than at 0.5 or 0.6 V. Concurrently, the formate band intensity increases rapidly after the potential step, reaching its maximum intensity within 20 s, which mirrors the decay of the CO_L signal. Subsequently, its intensity does not change much with time. With increasing temperature the steady-state formate band intensity decreases at this potential.

The general behavior, that is, the faster decrease of the CO intensity at higher electrode potentials and/or higher temperatures, reflects an increasing net rate for CO_{ad} removal by oxidation to CO_2 via electrochemical and/or thermal activation. A quantitative evaluation of the time-dependent changes in CO_{ad} coverage will be given in the next section.

In the above measurements, the electrocatalytic activity of the Pt electrode toward formic acid oxidation is reduced by the CO adlayer accumulated before the potential step. In the second set of potentiostatic experiments, the potential was stepped from 1.2 V to the same reaction potentials as used above, after it was held for 1 min at 1.2 V. This ensured that the initial amount of PtO_x species was similar in all measurements and that adsorbed CO and formate species are completely removed before the electrode potential was stepped back to lower values. After stepping from 1.2 to 0.5 V at 25 °C, both the CO_L and CO_M band intensities increase slowly with time but do not saturate within 2 min (Figure 6). The CO_{ad} band intensity clearly increases with temperature, reflecting the thermal activation of the dehydration of formic acid to CO_{ad}. On the other hand, the decreasing CO_L intensity for increasing reaction temperature observed upon stepping from 0.05 to 0.5 V points to an increasing CO_{ad} oxidation rate with temperature. (The other possibility, a decrease in CO_{ad} formation rate with temperature, which could equally explain these findings, appears to be unlikely.) The data demonstrate that under present reaction conditions, at 0.5 V, formic acid dehydration is much faster than CO_{ad} oxidation. Due to the slow reaction kinetics, the system has not yet reached steady-state conditions after 2 min, at least not for the lower temperatures (25−60 °C). (Therefore, the Faradaic current under "steady-state" conditions will be estimated by averaging over the current values in up-step and down-step experiments, as described below.) Finally, the formate band steeply increases to a temperature-dependent maximum value right after the potential step and then decays steadily with time. Both maximum and steady-state formate intensities decrease with increasing temperature. The later decay is tentatively attributed to a displacement of adsorbed formate by adsorbing CO.

When stepping the potential from 1.2 to 0.6 V, the time dependence of the CO_L and formate signals is quite similar to that obtained at 0.5 V. The intensities of the CO_L signals are, however, much smaller, while those of the formate species are slightly higher. Finally, when stepping the potential from 1.2 to 0.75 V, the CO_{ad} related signals are barely detectable at all temperatures. Also, formate shows slightly smaller intensities than those at 0.6 V, probably due to increasing competition with OH_{ad} adsorption/formation. Again, we find an increase of the formate band intensity with decreasing temperature, similar to the observations in the potentiodynamic measurements in Figures 2 and 3.

4. Discussion

Generally, the kinetics of electrochemical reactions are determined from the Faradaic current, which restricts these

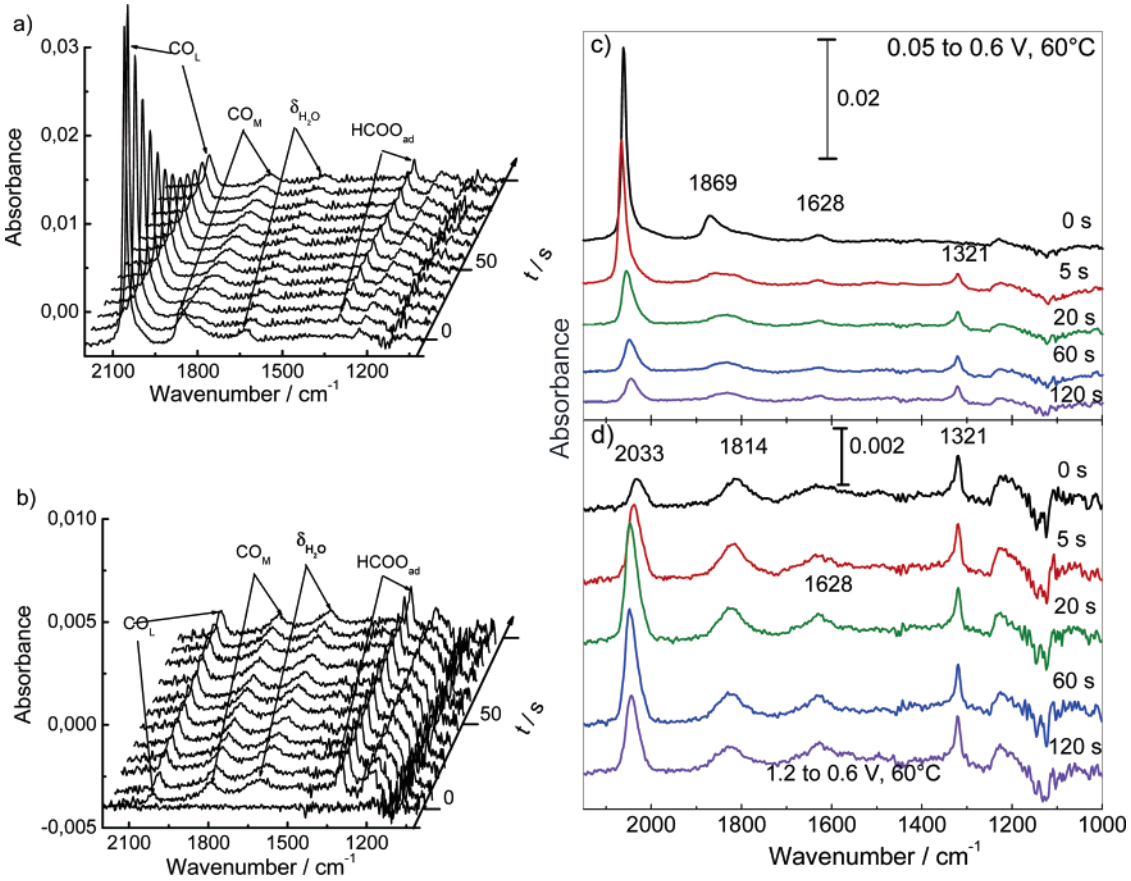

Figure 5. IR spectra of the Pt thin-film electrode in 0.1 M HCOOH + 0.5 M H_2SO_4 solution at 60 °C as a function of time after a potential step from (a) 0.05 to 0.6 V and (b) 1.2 to 0.6 V. Selected spectra at some specified times after the potential step from 0.05 to 0.6 V (c) and from 1.2 to 0.6 V (d).

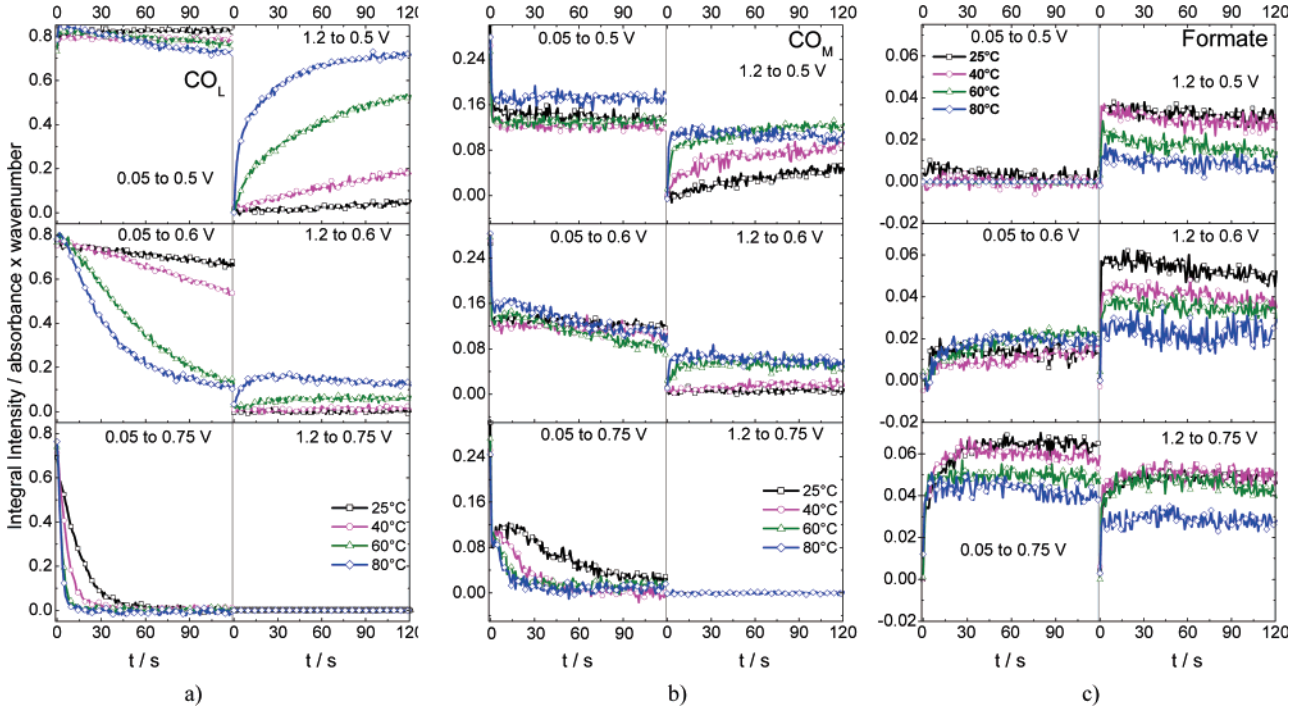

Figure 6. Evolution of the (a) CO_L, (b) CO_M, and (c) formate integral band intensities with time after the potential step at different temperatures. The other conditions are the same as those in Figure 4.

evaluations to the determination of effective rates and kinetic parameters for the entire, more complex reaction process. In the following, we will derive kinetic information for different partial reactions from the intensity−time profiles of the CO_{ad} band intensities. The change of CO_{ad} coverage can be written as the difference of the rates for CO_{ad} formation, r_1, and

oxidation, r_2

$$\frac{d\theta_{CO}}{dt} = r_1 - r_2 = k_1\theta_{HCOOH} - k_2\theta_{CO}\theta_{OH} \quad (1)$$

Here, k_1 denotes the rate constant for dehydration of a weakly adsorbed molecular formic acid precursor species to CO_{ad}, while k_2 is the rate constant for CO_{ad} oxidation to CO_2. Under steady-state conditions, we can set eq 1 to zero. The rate constants k_1 and k_2 will depend not only on the potential but, due to adsorbate−adsorbate interactions, also on the density and composition of the adlayer, making a comprehensive description of the reaction kinetics very complex. The IR data discussed above allow a kinetic evaluation in two situations: in the limit of negligible CO_{ad} coverages and in the limit of a saturated CO adlayer, where saturation refers to the saturation coverage obtained via formic acid adsorption (0.52 ML[44,67]). Specifically, we will investigate the following partial reactions: (i) the formation of CO_{ad} via dissociative adsorption (dehydration) of formic acid on a bare Pt surface at 0.5 and 0.6 V and (ii) the oxidation of CO_{ad} on a CO_{ad} covered Pt surface at different potentials (0.5, 0.6, and 0.75 V).

(i) HCOOH Dehydration to CO_{ad} at 0.5 and 0.6 V. The initial slope of the intensity−time curve for the CO_{ad} band obtained within the very first few seconds (or minute at lower temperatures) immediately after the potential step from 1.2 to 0.5 V is proportional to the rate for CO_{ad} formation via formic acid dehydration (r_1) on a CO_{ad}-free surface. The implicit assumption of negligible contributions from CO_{ad} oxidation under these conditions can be justified by the relatively low rate constant k_2 for CO_{ad} electrooxidation at 0.5 V and room temperature.[30,31] In addition, also, the CO_{ad} coverage right after the potential step is negligible.

For the calculation of reaction rates from the time dependence of the CO_{ad} related IR intensities, these were converted into CO_{ad} coverages, by performing a systematic set of calibration measurements. To account for any effects related to the origin of the CO adlayer, we followed the IR signals during adsorption from 0.01 M HCOOH for different times at 0.4 V and subsequently determined the resulting CO_{ad} coverage by CO_{ad} stripping (for details see ref 44). On the basis of these data, the ratio of CO_L and CO_M population varies with coverage, with only CO_M species present at the lowest CO_{ad} coverages, up to 0.09 ML, and an increasing population of CO_L species at higher coverages. The CO_{ad} coverage can be approximated by the following relations: In the low coverage range ($0 < \theta_{CO} \leq 0.29$ ML), it scales linearly with the integrated CO_M intensity, I_{CO_M}, via $\theta_{CO} = 1.69 \times I_{CO_M}$, and in the low and medium coverage ranges, it is linearly related to the CO_L intensity via $\theta_{CO} = 0.09 + 0.95 \times I_{CO_L}$ (0.09 ML $< \theta_{CO} \leq$ 0.25 ML) and via $\theta_{CO} = 0.18 + 0.4 \times I_{CO_L}$ (0.25 ML $< \theta_{CO} \leq$ 0.52 ML). The integrated intensities I_{CO_M} and I_{CO_L} are given in units of absorbance × wavenumber. These relations reproduce findings from previous reports[57,68] on the θ_{CO}−IR intensity relation on a qualitative scale but show differences upon quantitative comparison. Most important, the change in the relative CO_M and CO_L populations in the low coverage range, which prohibits a strictly proportional relation over the entire low and medium coverage ranges, differs from previous reports of a linear intensity−coverage relation over the low and medium coverage ranges, starting at $\theta_{CO} = 0$.[68]

The initial rate for formic acid dehydration to CO_{ad}, in the limits of zero CO_{ad} coverage ($r_2 = 0$) and normalized to the available surface sites (turnover frequency, TOF), can be calculated via the relation

$$\left[\frac{r_1}{N_{Pt}}\right]_{t=0} = TOF_{t=0} = \left[\frac{d\theta_{CO}}{dt}\right]_{t=0} = \left[\frac{d\theta_{CO_M}}{dt}\right]_{t=0} = 1.69\left[\frac{dI_{CO_M}}{dt}\right]_{t=0} \quad (2)$$

N_{Pt} describes the density of Pt surface atoms/cm^2 (1.3×10^{15} atoms·cm^{-2} for polycrystalline Pt), and dI_{CO_M}/dt is derived from the slope in the CO_M band intensity time curve right after the potential step from 1.2 V to the respective lower potentials (Figure 6). The CO_{ad} coverage is given in monolayers [ML], where 1 ML corresponds to one CO_{ad} per Pt surface atom. This way, we obtain a turnover frequency of 1.1×10^{-3} molecules·site^{-1}·s^{-1} at 0.5 V and 25 °C. This result is of similar order as the rate we observed in recent potentiostatic electrolyte exchange measurements in a flow-cell setup for the same parameters (1.8×10^{-3} molecules site^{-1}s^{-1}),[44] the remaining difference is most likely caused by a lower mass transport in the present setup without forced electrolyte flow, and agrees quite well with the values reported for formic acid decomposition on Pt single crystalline electrodes at similar potentials and room temperature by Sun et al.[20] By the use of the above density of Pt surface atoms, this turnover frequency corresponds to a rate of 2.4×10^{-3} nmol·cm^{-2}·s^{-1}. With increasing temperature, the dehydration rate increases to 7.2×10^{-3}, 3.1×10^{-2}, and 1.1×10^{-1} molecules·site^{-1}·s^{-1} at 40, 60, and 80 °C, respectively. Note that these rates are about a factor of hundred higher than the rates for CO_{ad} oxidation at the same potential at 60 and 80 °C on a CO_{ad} covered (0.52 ML) surface (see below). The temperature dependence of the formic acid dehydration rates (in TOFs) is plotted vs $1/T$ in the Arrhenius plot in Figure 7. From 25 to 80 °C, the dehydration rate increases by a factor of about 150, which leads to an apparent activation energy of 73 kJ·mol^{-1} for formic acid dehydration under the present conditions.

A similar evaluation of the initial slopes of the CO_{ad} related intensities was performed at 0.6 V, which lead to TOFs of 3.3×10^{-5}, 1.8×10^{-4}, 4.3×10^{-3}, and 4.4×10^{-2} molecules·site^{-1}·s^{-1} at 25, 40, 60, and 80 °C, respectively. These values and the related rates are given in Table 1. Also, in this case,

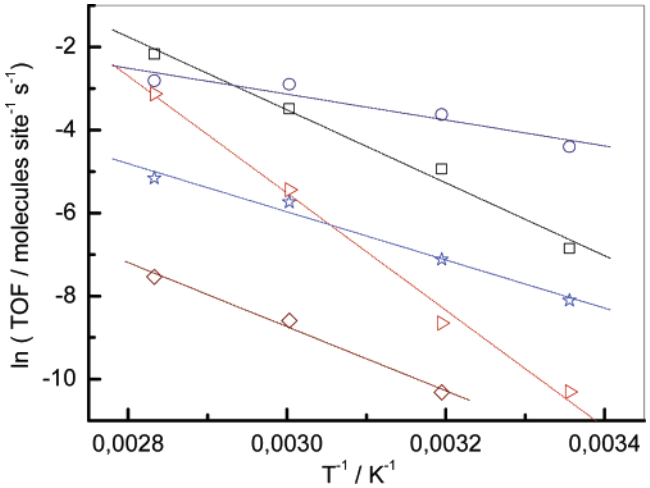

Figure 7. Arrhenius plot of the (initial) rates for formic acid dehydration, in the limits of very low CO_{ad} coverages, at 0.5 V (squares) (a) and at 0.6 V (triangles) (b), and of the initial rates for CO_{ad} oxidation on a CO_{ad} saturated surface (ca. 0.52 ML CO_{ad}) at (c) 0.5 V (diamonds), (d) 0.6 V (stars), and (e) 0.75 V (circles).

TABLE 1: Rates of Formic Acid Dehydration on a CO_{ad} Free Pt Surface and for CO_{ad} oxidation on a CO_{ad} Saturated Surface[a]

reaction temperature	HCOOH dehydration ($\theta_{CO} = 0$)/ molecule·site^{-1}·s^{-1}		CO_{ad} oxidation ($\theta_{CO} = 0.52$)/ molecule·site^{-1}·s^{-1}		
	0.5 V	0.6 V	0.5V	0.6 V	0.75 V
25 °C	1.1×10^{-3}	3.3×10^{-5}	0	3.0×10^{-4}	1.2×10^{-2}
40 °C	7.2×10^{-3}	1.8×10^{-4}	3.3×10^{-5}	8.1×10^{-4}	2.6×10^{-2}
60 °C	3.1×10^{-2}	4.3×10^{-3}	1.9×10^{-4}	3.2×10^{-3}	5.5×10^{-2}
80 °C	1.1×10^{-1}	4.4×10^{-2}	5.3×10^{-4}	5.7×10^{-3}	6.0×10^{-2}

[a] The rates for formic acid dehydration on the "CO_{ad} free" surface ($\theta_{CO} \approx 0$) were derived from the net increase in CO_{ad} related IR intensity upon stepping from 1.2 V to the respective reaction potential, those for CO_{ad} oxidation on the CO_{ad} saturated surface ($\theta_{CO} \approx 0.52$ ML) were determined from the decay in CO_{ad} related IR intensity upon stepping from 0.05 V to the respective reaction potential.

TABLE 2: Activation Energies E_a^i Derived from the CO_{ad} Band Intensity−Time Profiles in Figures 6 and 7[a]

	HCOOH dehydration ($\theta_{CO} \approx 0$)		CO_{ad} oxidation ($\theta_{CO} \approx 0.52$)		
potential/V	0.5	0.6	0.5	0.6	0.75
E_a^i/kJ·mol^{-1}	73	117	64	48	26

[a] Energy values derived upon stepping from 1.2 V to the respective reaction potentials are denoted as $\theta_{CO} \approx 0$, while those obtained upon stepping from 0.05 V to the reaction potential are denoted as $\theta_{CO} \approx$ 0.52 ML.

the value at 25 °C is somewhat lower than that obtained in the flow-cell experiment mentioned above,[44] which is explained by the same reason. A plot of these TOFs in the Arrhenius diagram in Figure 7 results in an activation energy for HCOOH dehydration under these conditions of 117 kJ·mol^{-1}. It has to be noted, however, that at 0.6 V the tacit assumption of negligible CO_{ad} oxidation rates, at least compared with the rates for CO_{ad} formation, may no longer be justified, at least not without further considerations. In that sense, the above rates for formic acid dehydration (at 0.6 V) and the related activation energy are effective values, possibly including contributions from CO_{ad} oxidation, as given by eq 1, and the actual rate for HCOOH dehydration is described by the sum of the experimentally determined increase in CO coverage and the CO_{ad} oxidation rate. Considering that we evaluate the rates in the limits of $\theta_{CO} \approx 0$, contributions from the CO_{ad} oxidation rate are expected to be small, as concluded from measurements of the CO_{ad} oxidation rate at low CO_{ad} coverage at this potential, but have to be kept in mind. This effect, in combination with the lower barrier and hence less pronounced temperature dependence of the CO_{ad} oxidation rate (see below), can result in a higher measured (apparent) activation energy than the actual value, which may at least partly explain the higher value of 117 kJ·mol^{-1}.

(ii) CO_{ad} Oxidation on the CO_{ad} Covered Surface. Next, we can determine the rate for CO_{ad} oxidation at different potentials (0.5, 0.6 and 0.75 V) on a CO_{ad} saturated surface, where saturation refers to the saturation level obtained by formic acid dehydrogenation under the present conditions (ca. 0.52 ML[44]), and therefore further HCOOH dehydration is not possible. In this case, we can determine the CO_{ad} oxidation rate from the initial slope of the intensity decay of the CO_{ad} related CO_L signal, right after stepping the potential from 0.05 V to the respective reaction potential. The resulting TOFs are compiled in Table 1. The CO_{ad} oxidation rate rises by about 2 orders of magnitude when increasing the reaction potential from

TABLE 3: Quasi Steady-state Faradaic Current Densities[a]

	current density/mA·cm^{-2}		
	0.5 V	0.6 V	0.75 V
25 °C	0.068	0.097	0.15
40 °C	0.12	0.17	0.20
60 °C	0.22	0.45	0.42
80 °C	0.36	0.74	0.82
activation energy/kJ·mol^{-1}	26	33	27

[a] Quasi steady-state currents are measured in the potential-step experiments 2 min after the potential step, averaged over up-step and down-step experiments (see Figure 4), that is, close to steady-state conditions at the respective potential.

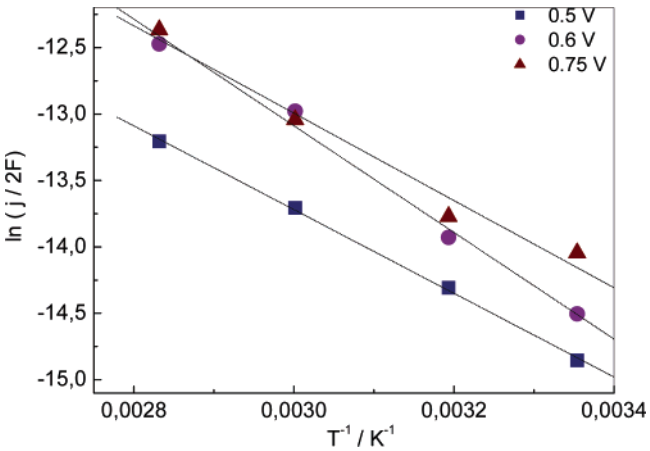

Figure 8. Arrhenius plot of the steady-state rates for formic acid oxidation at different potentials deduced from the Faradaic currents in the potentiostatic measurements (see Table 3).

0.5 to 0.75 V at the same temperature. On the other hand, at constant potential, the increase in temperature, from 25 to 80 °C, results in an increase of the initial CO_{ad} oxidation rate by about a factor of 4. The temperature dependence of these rates is equally plotted in the Arrhenius diagram in Figure 7. From the slopes of the ln(TOF) vs $1/T$ plots, we derive apparent activation energies of 64, 48, and 26 kJ·mol^{-1} for CO_{ad} oxidation on a CO_{ad} saturated surface at 0.5, 0.6, and 0.75 V, respectively. Tentatively, we attribute the decrease of the activation energy for CO_{ad} oxidation with increasing potential to a decrease in the energy for OH_{ad} formation at higher potentials, due to a stabilization of the OH_{ad} with increasing potential. In that case, OH_{ad} formation (or reaction of OH_{ad} with CO_{ad}) is rate limiting, which at the high CO_{ad} coverage in these experiments appears plausible.

Finally, we also calculated the effective activation energy E_a^i for the total reaction from the steady-state Faradaic currents. Here, it is important to realize that this is an effective value, since the measurements at different temperatures are likely to lead to different steady-state adlayer coverages, which in turn will also affect the Faradaic current. The steady-state current densities at different potentials are determined by averaging over the current densities obtained in the up-step and down-step potential-step experiments after 2 min. These steady-state rates are compiled in Table 3 and plotted in the Arrhenius diagram in Figure 8; the resulting effective activation energies are collected in Table 3.

These effective activation energies for formic acid oxidation can be compared with results on Pt electrodes in previous studies. Fleischmann et al. reported a decrease of the Tafel slope with increasing temperature and an effective activation energy of 50 kJ·mol^{-1} at 0.5 V.[46] Later on, Murugkar and Lal derived

an activation energy of 38 kJ·mol^{-1} at the same potential from rotating disk electrode (RDE) measurements in 0.5 M HCOOH + 0.5 M H_2SO_4 solution, which is quite close to the present values.[48] Furthermore, these authors observed a decay of the activation energy with increasing potential. Sun et al. determined effective standard activation energies in the range from 10 to 32 kJ·mol^{-1} for the reaction in 0.005 M HCOOH solution at 0.25 V on 5 different index Pt single crystalline surfaces.[49] Values of 53 kJ·mol^{-1} at 0.65 V and 83 kJ·mol^{-1} at 0.5 V were reported by Schmidt et al. from potentiostatic RDE experiments for formic acid oxidation on Pt(111) in 0.05 M HCOOH + 0.5 M $HClO_4$ solution.[22] Jiang et al. determined activation energies of 58.7 and 45.1 kJ·mol^{-1} at 0.376 and 0.276 V, respectively, for formic acid oxidation on Pt nanoparticles in 0.5 M HCOOH + 0.5 M H_2SO_4 solution.[24] The relatively large spread of the effective activation energies in these different measurements can at least partly be explained by the variation in HCOOH concentration,[24] base electrolyte (anion effects[69]), and of the respective reaction potential, indicating that the condition of the catalyst, in particular the respective adsorbate coverages, will sensitively affect the activation energy. But even for comparable conditions the data scatter considerably, see, for example, the results of Murugkar and Lal[48] and Jiang et al.,[24] which were both measured in 0.5 M HCOOH + 0.5 M H_2SO_4 solution. Nevertheless, concentrating on similar reaction conditions, the present values for the effective activation energy fit well into the sequence of activation energies. Apparent activation energies for the partial reactions contributing to formic acid oxidation, as derived here from the IR intensities, have not been reported so far.

Next, we want to discuss the question of the relative contribution of the two reaction pathways to the total formic acid oxidation rate. Taking the data at 0.6 V as an example and using the high-coverage CO_{ad} oxidation rate (after the step from 0.05 to 0.6 V) as a rough estimate, a CO turnover rate of 3×10^{-4} molecules·site^{-1}·s^{-1} at 25 °C (5.7×10^{-3} molecules·site^{-1}·s^{-1} at 80 °C) corresponds to a Faradaic current of 0.13 μA·cm^{-2} (2.4 μA·cm^{-2} at 80 °C) for CO oxidation to CO_2. The measured Faradaic current density, however, is around 0.097 mA·cm^{-2} at 25 °C (0.74 mA·cm^{-2} at 80 °C). Hence, for a reaction at 25 °C and at 0.6 V, the total Faradaic current measured is almost 3 orders of magnitude larger than the current from CO_{ad} oxidation as deduced from the IR results. At 80 °C and at 0.6 V, CO_{ad} oxidation ("indirect pathway") contributes less than 1% to the total anodic current. Thus, the contribution of the indirect pathway to the total anodic current increases with temperature.

At 0.75 V, the differences between the values determined this way for the CO_{ad} oxidation rate and the rates under steady-state conditions are significantly higher than those at the lower potentials due to the negligible steady-state CO_{ad} coverages. Therefore, the rates for CO_{ad} oxidation on a CO_{ad} saturated surface, which were derived upon stepping from 0.05 to 0.75 V (TOFs of 0.012, 0.026, 0.055 and 0.06 molecules·site^{-1}·s^{-1} at 25, 40, 60, and 80 °C, respectively), are significantly higher than the steady-state rates. (It should be noted that the CO_{ad} oxidation rate decreases with decreasing CO_{ad} coverage under present conditions, as evidenced by the shape of the intensity−time profiles in Figure 6.) Accordingly, the contribution of the indirect pathway, via formation and oxidation of CO_{ad}, is expected to be much smaller than the values of below 5% calculated from comparing the Faradaic currents corresponding to CO_{ad} oxidation (see Table 3) with the measured total anodic current (0.15, 0.2, 0.42, and 0.82 mA·cm^{-2}) determined under steady-state conditions at 0.75 V.

From the above discussion, we can conclude that the "direct" pathway, not involving CO_{ad} formation and oxidation, represents the dominant reaction pathway at all potentials and temperatures investigated here, contributing by more than 95% at 0.75 V and by more than 99% at potentials ≤0.6 V to the total formic acid oxidation rate in the entire temperature range. At potentials cathodic of the lower limit of the present study, we expect the contribution of the indirect pathway to be even lower, because of the very low CO_{ad} oxidation rates under these conditions. Hence, at potentials relevant for fuel cell operations, the indirect pathway, via formation and oxidation of CO_{ad}, is a clear minority pathway.

Finally, we want to briefly discuss the role of adsorbed formate in the dominant direct pathway. It is clear from these and recent IR spectroscopic data[40] that adsorbed formate species are involved in formic acid oxidation as stable adsorbed reaction intermediates. It is not clear, however, whether their formation and oxidative decomposition to CO_2 and H^+ is rate determining. If this is the case, then they would represent the reactive intermediate in the majority reaction pathway. If not, then this would require an additional, dominant reaction pathway. In this context, it is of interest that in contrast to the increase of the steady-state anodic current for formic acid oxidation with temperature the intensity of the formate band and hence also the formate coverage decreases with increasing temperature. If the formation and oxidation of adsorbed formate is rate limiting and hence represents the dominant, majority reaction pathway, then this observation can only be explained if the increase in the formate oxidation rate with temperature is faster than that for formate formation, that is, the activation energy for formate formation (formic acid dehydrogenation) must be lower than that for the oxidative decomposition of adsorbed formate. These questions on the nature of the dominant reaction pathway and on the role of the adsorbed formate species therein have been investigated in refs 44 and 45.

5. Summary

The electrooxidation of HCOOH on a Pt electrode in sulfuric acid solution has been studied by a combination of electrochemical and in-situ ATR-FTIR spectroscopy measurements, under both potentiodynamic and potentiostatic conditions, at temperatures between 25 and 80 °C. On the basis of the IR spectra, CO_{ad} and bridge-bonded $HCOO_{ad}$ are the only formic acid related adsorbates on the Pt electrode surface detectable at all reaction conditions. The intensity of the CO_{ad} signal increases and that of adsorbed formate decreases with temperature, indicating a faster dehydration of formic acid to CO_{ad} and formate consumption/desorption at higher temperatures relative to formate adsorption. The rates of the individual reactions for CO_{ad} formation (formic acid dehydration) in the limit of very low CO_{ad} coverages (0.5, 0.6 V) as well as for CO_{ad} oxidation at saturation coverage (0.5, 0.6 and 0.75 V) were derived from the initial slopes of the intensity−time profiles of the IR bands related to CO_{ad} in adsorption/reaction transients, making use of the calibrated relation between IR intensity and CO_{ad} coverage in the coverage range between 0 and 0.52 ML determined previously.[44] From the temperature dependence of the above rates, we obtained activation energies for the individual reactions described above; measurements of the Faradaic currents under steady-state conditions result in apparent activation energies for the total reaction.

At potentials up to 0.5 V, the rate of formic acid dehydration (CO_{ad} formation), in the limit of very low CO_{ad} coverages, is

much higher than that for CO_{ad} oxidation, in the limit of CO_{ad} saturation, over the entire temperature range from 25 to 80 °C, which leads to CO_{ad} accumulation on the surface. At higher potentials or lower temperatures, CO_{ad} oxidation becomes increasingly faster compared with the increase in CO_{ad} formation rate, resulting in lower steady-state CO_{ad} coverages.

The effective activation energies of the total process under steady-state conditions, E_a^i, derived from the quasi steady-state Faradaic currents, are significantly lower than the barrier for CO oxidation under comparable conditions, indicating that CO_{ad} oxidation is not the rate-limiting step in the majority reaction path. This is confirmed by comparing the partial reaction current for CO_{ad} oxidation calculated from the IR based CO_{ad} oxidation rates with the total Faradaic current. At 0.6 and 0.75 V, the indirect pathway contributes to less than 1% and less than 5%, respectively, to the total Faradaic reaction current for HCOOH oxidation to CO_2. At the higher potential, the indirect pathway is limited by the slow HCOOH dehydration (CO_{ad} formation). The contribution of the indirect pathway increases with temperature, reflecting its higher activation barrier compared with the total reaction, but even at 80 °C and 0.6 V it contributes less than 1%, making the direct pathway by far the dominant one under the reaction conditions in this study.

Finally, these results demonstrated the potential of this spectroscopy-based approach not only for identifying reaction intermediates and reaction pathways but also for the quantitative evaluation of the reaction rates of individual pathways and their activation energies. Similar strategies can be applied not only for studies of a wide range of electrocatalytic reactions but for reaction processes in general.

Acknowledgment. This work was supported by the Deutsche Forschungsgemeinschaft (Projects BE 1201-8/4 and BE 1201-11/1) and by the Forschungsallianz Brennstoffzellen Baden-Württemberg (FABZ). We are grateful to the Alexander von Humboldt Foundation for a fellowship for Y.X.C. and to the Ministry of Education, Culture, Sports, Science and Technology of Japan (MEXT) (Grant-in-aid for Basic Research No. 14205121 and for Scientific Research on Priority Areas 417) for support of the initial experiments.

References and Notes

(1) Osawa, M. *Bull. Chem. Soc. Jpn.* **1997**, *70*, 2861.
(2) Osawa, M. *Handbook of Vibrational Spectroscopy*; John Wiley & Sons: Chichester, U.K., 2002; pp 785−799.
(3) Iwasita, T.; Nart, F. C. *Prog. Surf. Sci.* **1997**, *55*, 271.
(4) Breiter, M. W. *J. Electroanal. Chem.* **1967**, *14*, 407.
(5) Capon, A.; Parsons, R. *J. Electroanal. Chem.* **1973**, *44*, 1.
(6) Capon, A.; Parsons, R. *J. Electroanal. Chem.* **1973**, *45*, 205.
(7) Parsons, R.; VanderNoot, T. *J. Electroanal. Chem.* **1988**, *257*, 9.
(8) Beden, B.; Léger, J.-M.; Lamy, C. *Modern Aspects of Electrochemistry*; Kluwer Adcademic/Plenum Publishers: New York, 1992; pp 97−263.
(9) Jarvi, T. D.; Stuve, E. M. *Electrocatalysis*; Wiley-VCH: Heidelberg, Germany, 1998; pp 75−153.
(10) Sun, S.-G. *Electrocatalysis*; Wiley-VCH: New York, 1998; pp 243−290.
(11) Hamnett, A. *Interfacial Electrochemistry: Accomplishments and Challenges*; Marcel Dekker Inc.: New York, 1999; pp 843−883.
(12) Markovic, N. M.; Ross, P. N., Jr. *Surf. Sci. Rep.* **2002**, *45*, 117.
(13) Wasmus, S.; Wang, J.-T.; Savinell, R. F. *J. Electrochem. Soc.* **1995**, *142*, 3825.
(14) Fan, Q.; Pu, C.; Smotkin, E. S. *J. Electrochem. Soc.* **1996**, *143*, 3053.
(15) Lin, W.-F.; Wang, J.-T.; Savinell, R. F. *J. Electrochem. Soc.* **1997**, *144*, 1917.
(16) Sanicharane, S.; Bo, A.; Sompalli, B.; Gurau, B.; Smotkin, E. S. *J. Electrochem. Soc.* **2002**, *149*, A554.
(17) Tkach, I.; Panchenko, A.; Kaz, T.; Gogel, V.; Friedrich, K. A.; Roduner, E. *Phys. Chem. Chem. Phys.* **2004**, *6*, 5419.
(18) Rice, C.; Ha, S.; Masel, R. I.; Wieckowski, A. *J. Power Sources* **2003**, *115*, 229.
(19) Zhu, Y.; Ha, S.; Masel, R. I. *J. Power Sources* **2004**, *130*, 8.
(20) Sun, S.-G.; Lin, Y.; Li, N.-H.; Mu, J.-Q. *J. Electroanal. Chem.* **1994**, *370*, 273.
(21) Weber, M.; Wang, J.-T.; Wasmus, S.; Savinell, R. F. *J. Electrochem. Soc.* **1996**, *143*, L158−L160.
(22) Schmidt, T. J.; Behm, R. J.; Grgur, B. N.; Markovic, N. M.; Ross, P. N. *Langmuir* **2000**, *16*, 8159.
(23) Yang, Y.-Y.; Zhou, Z.-Y.; Sun, S.-G. *J. Electroanal. Chem.* **2001**, *500*, 233.
(24) Jiang, J.; Kucernak, A. *J. Electroanal. Chem.* **2002**, *520*, 64.
(25) Nonaka, H.; Matsumura, Y. *J. Electroanal. Chem.* **2002**, *520*, 101.
(26) Lin, W. F.; Christensen, P. A.; Hamnett, A. *Phys. Chem. Chem. Phys.* **2001**, *3*, 3312.
(27) Capon, A.; Parsons, R. *J. Electroanal. Chem.* **1973**, *44*, 239.
(28) Watanabe, M.; Motoo, S. *Denki Kagaku* **1973**, *41*, 190.
(29) Wolter, O.; Willsau, J.; Heitbaum, J. *J. Electrochem. Soc.* **1985**, *132*, 1635.
(30) Markovic, N. M.; Schmidt, T. J.; Grgur, B. N.; Gasteiger, H. A.; Behm, R. J.; Ross, P. N. *J. Phys. Chem. B* **1999**, *103*, 8568.
(31) Anderson, A. B. *Electrochim. Acta* **2002**, *47*, 3759.
(32) Note that this CO adlayer was prepared by HCOOH decomposition and that the saturation coverage accessible by formic acid oxidation is much lower than what can be reached by adsorption from gas-phase CO, namely, 0.52 monolayers (ML) instead of 0.75 ML in the latter case.
(33) Corrigan, D. S.; Weaver, M. J. *J. Electroanal. Chem.* **1988**, *241*, 143.
(34) Xia, X.; Iwasita, T.; Vielstich, W. *Electrochemistry* **1997**, *3*, 26.
(35) Sun, S.-G.; Clavilier, J.; Bewick, A. *J. Electroanal. Chem.* **1988**, *240*, 147.
(36) Beden, B.; Bewick, A.; Lamy, C. *J. Electroanal. Chem.* **1983**, *148*, 147.
(37) Kunimatsu, K.; Kita, H. *J. Electroanal. Chem.* **1987**, *218*, 155.
(38) Iwasita, T.; Xia, X.; Herrero, E.; Liess, H.-D. *Langmuir* **1996**, *12*, 4260.
(39) Gomez, R.; Weaver, M. J. *J. Electroanal. Chem.* **1997**, *435*, 205.
(40) Miki, A.; Ye, S.; Osawa, M. *Chem. Commun.* **2002**, 1500.
(41) Columbia, M. R.; Crabtree, A. M.; Thiel, P. A. *J. Am. Chem. Soc.* **1992**, *114*, 1231.
(42) Chen, Y.-X.; Miki, A.; Ye, S.; Sakai, H.; Osawa, M. *J. Am. Chem. Soc.* **2003**, *125*, 3680.
(43) Miki, A.; Ye, S.; Sensaki, T.; Osawa, M. *J. Electroanal. Chem.* **2004**, *563*, 23.
(44) Chen, Y.-X.; Heinen, M.; Jusys, Z.; Behm, R. J. *Angew. Chem., Int. Ed.* **2006,** *45*, 981.
(45) Samjeske, G.; Osawa, M. *Angew. Chem., Int. Ed.* **2005**, *44*, 5694.
(46) Fleischmann, C. W.; Johnson, G. K.; Kuhn, A. *J. Electrochem. Soc.* **1964**, *111*, 602.
(47) Meenakahisundaram, N.; Vassilyev, Y. B.; Bagotzky, V. S. *Elektrokhimiya* **1967**, *3*, 193.
(48) Murugkar, V. L.; Lal, H. *J. Electroanal. Chem.* **1977**, *77*, 299.
(49) Sun, S.-G.; Yang, Y.-Y. *J. Electroanal. Chem.* **1999**, *467*, 121.
(50) Okamoto, H.; Kon, W.; Mukouyama, Y. *J. Phys. Chem. B* **2004**, *108*, 4432.
(51) Ataka, K.; Yotsuyangi, T.; Osawa, M. *J. Phys. Chem. B* **1996**, *100*, 10664.
(52) Angerstein-Kozlowska, H.; Conway, B. E.; Sharp, W. B. A. *J. Electroanal. Chem.* **1973**, *43*, 9.
(53) Markovic, N.; Ross, P. N. *J. Electroanal. Chem.* **1992**, *330*, 499.
(54) Iwasita, T.; Xia, X.; Liess, H.-D.; Vielstich, W. *J. Phys. Chem. B* **1997**, *101*, 7542.
(55) Strasser, P.; Lübke, M.; Raspel, F.; Eiswirth, M.; Ertl, G. *J. Chem. Phys.* **1997**, *107*, 979.
(56) Willsau, J.; Heitbaum, J. *Electrochim. Acta* **1986**, *31*, 943.
(57) Kunimatsu, K. *J. Electroanal. Chem.* **1986**, *213*, 149.
(58) Lu, G. Q.; Crown, A.; Wieckowski, A. *J. Phys. Chem. B* **1999**, *103*, 9700.
(59) Bewick, A.; Pons, S. *Advances in Infrared and Raman Spectroscopy*; Wiley and Heyden: London, 1985; pp 1−63.
(60) Hahn, F.; Beden, B.; Lamy, C. *J. Electroanal. Chem.* **1986**, *204*, 315.
(61) Futamata, M.; Luo, L.; Nishihara, C. *Surf. Sci.* **2005**, *590*, 196.
(62) Oxley, J. E.; Johnson, G. K.; Buzalski, B. T. *Electrochim. Acta* **1964**, *9*, 897.
(63) Jusys, Z.; Behm, R. J. *J. Phys. Chem. B* **2001**, *105*, 10874.
(64) Vielstich, W. *Encyclopedia of Electrochemistry, Interfacial Kinetics and Mass Transport*; Wiley-VCH: Weinheim, Germany, 2003; Vol. 2.
(65) Podlovchenko, B. I.; Manzhos, R. A.; Maksimov, Y. M. *Electrochim. Acta* **2005**, *50*, 4807.
(66) Chen, Y.-X.; Jusys, Z.; Behm, R. J. Unpublished results.
(67) Jusys, Z.; Behm, R. J. To be submitted for publication.
(68) Chang, S. C.; Weaver, M. J. *J. Phys. Chem.* **1990**, *92*, 2, 4582.
(69) Kumara Swamy, B. E.; Maye, J.; Vannoy, C.; Schell, M. *J. Phys. Chem. B* **2004**, *108*, 16488.